Fuel 87 (2008) 3040–3045

Contents lists available at ScienceDirect

Fuel

journal homepage: www.fuelfirst.com

Adsorption of an acid dye onto coal fly ash

Ting-Chu Hsu *

Department of Environmental Engineering, Vanung University, Chung-Li 320, Taiwan

ARTICLE INFO

Article history:
Received 1 August 2007
Received in revised form 26 January 2008
Accepted 29 March 2008
Available online 24 April 2008

Keywords:
Coal fly ash
AR1
Kinetic

ABSTRACT

In this study, we found the raw coal fly ash (CFA) that had not been subjected to any pretreatment process had superior adsorbing ability for the anionic dye Acid Red 1 (AR1) than did two modified coal fly ashes (CFA-600 and CFA-NaOH). The adsorption capacities followed the order CFA > CFA-600 > CFA-NaOH, and they each increased upon increasing the temperature (60 °C > 45 °C > 30 °C). The adsorptions of AR1 onto CFA, CFA-600, and CFA-NaOH all followed pseudo-second-order kinetics. The isotherms for the adsorption of AR1 onto the raw and modified coal fly ashes fit the Langmuir isotherm quite well; the adsorption capacities of CFA, CFA-600, and CFA-NaOH for AR1 were 92.59–103.09, 32.79–52.63, and 12.66–25.12 mg g^{-1}, respectively. According to the positive values of $\Delta H°$ and $\Delta S°$, these adsorptions were endothermic processes. The ARE and EABS error function methods provided the best parameters for the Langmuir isotherms and pseudo-second-order equations, respectively, in the AR1–CFA adsorption system.

1. Introduction

The many industries that use dyes and pigments – such as those involving textiles, dying, and papermaking – discharge large amounts of colorful materials in their wastewater. Because these effluents can cause adverse effects such as allergic dermatitis, skin irritation, cancer, and mutation [1], it is imperative to remove these dye pollutants from bodies of water. Various methods have been used for the treatment of dye-containing wastewater, including biological treatment, adsorption, chemical oxidation, coagulation, and reverse osmosis [2,3]. Although activated carbon adsorption is highly effective at removing dyes and pigments, it is often too expensive to be used in developing countries; in such cases, the use of low-cost adsorbents, such as clay minerals [4], bottom and fly ash [5–12], fungi [13], waste materials from agriculture [14–18] and elsewhere [19–22], might be more appropriate. There are many reports describing the adsorption abilities of various fly ashes for the removal of dyes from water, but few studies have been performed to determine the kinetics of dye adsorption on fly ash [8]. One potential approach is the use of coal fly ash as a low-cost adsorbent.

In Taiwan, coal is used to generate almost 50% of the total electricity production; the amount of coal fly ash produced currently exceeds 1.6 million tons per year, and attempts are being made to reduce this volume of waste prior to disposal. Although coal fly ash is incorporated into cement and concrete as a structural filler and for waste and road base stabilization [23], it is unlikely that these applications will ever result in the consumption of all of the fly ash generated. Because coal fly ash is an efficient adsorbent of dyes and pigments, to increase its scope of application we investigated the use of raw and modified coal fly ashes for the removal of colored impurities from wastewater.

2. Materials and methods

2.1. Adsorbents

Raw coal fly ash (CFA) generated from a full-scale power-generating unit burning anthracite and bituminous coal was used in these experiments. The CFA was collected at the electrostatic precipitator (ESP); it contained SiO_2 (52.5%), Al_2O_3 (27.9), CaO (6.27%), MgO (1.6%), Fe_2O_3 (6.3%), SO_3 (0.79%), and LOI ("loss on ignition" – the unburned carbon portion in the sample; 5.01%); according to ASTM C618, this material can be classified as class F because it contained less than 10% CaO, 5% SO_3, and 12% LOI and greater than 70% of the three main components (SiO_2, Al_2O_3, and Fe_2O_3) combined.

One portion of the CFA sample was treated in a furnace at 600 °C for 4 h and then stored in a desiccator prior to use (CFA-600); the other portion was mixed with 6 N NaOH in a stainless-steel beaker and maintained at 90 °C for 0.5 h with stirring. The latter mixture was left for 4 h to settle the complexes, which were then dialyzed against distilled water (until the conductivity became less than 300 μS cm^{-1}), powdered, ground, and stored in a desiccator prior to use (CFA-NaOH).

2.2. Adsorbate

Acid Red 1 (AR1), an anionic dye supplied by Aldrich Chemical Co. (USA), was used as the adsorbate in this study. The structure

* Tel.: +886 3 434 2379x46; fax: +886 346 22232.
E-mail address: djshue@msa.vnu.edu.tw

0016-2361/$ - see front matter © 2008 Elsevier Ltd. All rights reserved.
doi:10.1016/j.fuel.2008.03.026

of AR1 is displayed in Fig. 1. AR1 has a maximum UV–Vis absorbance at a wavelength of 530 nm. An accurately weighed quantity of the dye was dissolved in distilled water to prepare a stock solution (1000 mg/L). Experimental solutions of the desired concentrations were obtained through successive dilutions with distilled water.

2.3. Adsorption measurements

XRD patterns of the CFA samples were measured using a wide-angle X-ray diffractometer (Thermo ARL X'TAR, Switzerland). The surface areas and total pore volumes of the CFA samples were measured through N_2 adsorption at 77 K using a Micromeritics TRISTAR-3000 apparatus (Particle & Surface Sciences Pty. Ltd., Australia). The chemical compositions of the CFA samples were measured using a Z-4100 inductively coupled plasma atomic emission spectroscope (Hitachi, Japan). The pH and conductivity were determined using a MODEL-1671 pH meter (JenCo, Taiwan). The zeta potential was determined using a Zetasizer Nano Series ZEN-3600 instrument (Malvern, UK). CFA-600 was treated at 600 °C in a TB50 furnace (SmartLab, Taiwan). The resulting suspensions were filtered and their concentrations of dye determined by recording the absorbance at the characteristic wavelength using a U-2000 UV–Vis spectrophotometer (Hitachi, Japan) and employing a calibration curve that correlated the absorbances to the concentrations of standard dye solutions. The adsorption capacity of dyes was then calculated from

$$Q_e = \frac{V\Delta C}{m}, \quad (1)$$

where V is the volume of the liquid phase, m is the mass of the solid, and ΔC is computed simply from the difference between the initial and final UV readings. For the adsorption kinetics experiments, the amounts of adsorbed dyes were determined by analyzing the solutions at appropriate time intervals.

2.4. Sorption studies

Adsorption kinetics and isotherm experiments for the various CFA samples were undertaken in a batch equilibrium system. The AR1 adsorption isotherms in aqueous solutions were obtained using the immersion method. Prior to their use, the adsorbents were dried at 105 °C for 24 h to remove traces of moisture. Dye solutions were prepared by dissolving AR1 in distilled water. For kinetics studies, the adsorption of AR1 was studied after adding the adsorbent (0.1 g) into an aqueous solution containing AR1 (400 mg/L) and shaking at 30 °C for various reaction times. The equilibrium, which was determined by dynamic adsorption studies, was established within 2–3 h; therefore, the contact time was fixed at 3 h. The adsorption isotherms of AR1 were studied after adding 0.1 g of an adsorbent into the aqueous solution containing a desired AR1 concentration (50–400 mg L^{-1}), and shaking at 200 rpm for 3 h at 30 °C in a reciprocating shaker (DengYng Z-901, Taiwan). For thermodynamic studies, these procedures were repeated at 45 and 60 °C. The pH of each solution was adjusted to a constant value of 6.0 through the addition of NaOH or HCl solution.

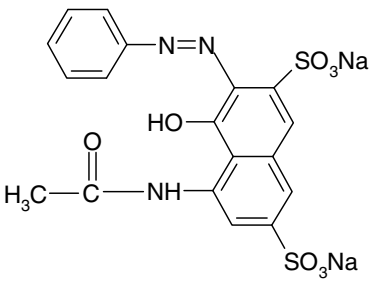

Fig. 1. Molecular structure of AR1.

3. Results and discussion

3.1. Characterization of adsorbents

The textural characteristics of fly ash are presented in Table 1 [24]. The BET surface areas increased in the order CFA-600 < CFA < CFA-NaOH; i.e., the same trend with regard to the pore volume. The presence of SiO_2(γ-quartz) and mullite was evident from the XRD patterns of the three adsorbents. In addition, the XRD patterns of CFA-NaOH indicated the presence of Na-A zeolite and hydroxysodalite [24].

3.2. Effect of zeta potential and pH

The surface charge–pH curves for CFA, CFA-600, and CFA-NaOH are provided in Fig. 2. The surface charge of CFA was positive at pH 6, implying that the ion-exchange process between AR1 and CFA was operative. On the other hand, the surface charges of CFA-600 and CFA-NaOH were almost neutral and negative, respectively, at

Table 1
Pore structure data and chemical phases for the CFA samples

Adsorbent	S_{BET} (m^2 g^{-1})	V_{total} (cm^3 g^{-1})	Pore diameter (nm)	Phases
CFA	9.21	0.020	8.54	γ-quartz, mullite
CFA-600	5.38	0.015	11.49	γ-quartz, mullite
CFA-NaOH	33.65	0.172	20.39	γ-quartz, mullite, Na-A zeolite, hydroxysodalite

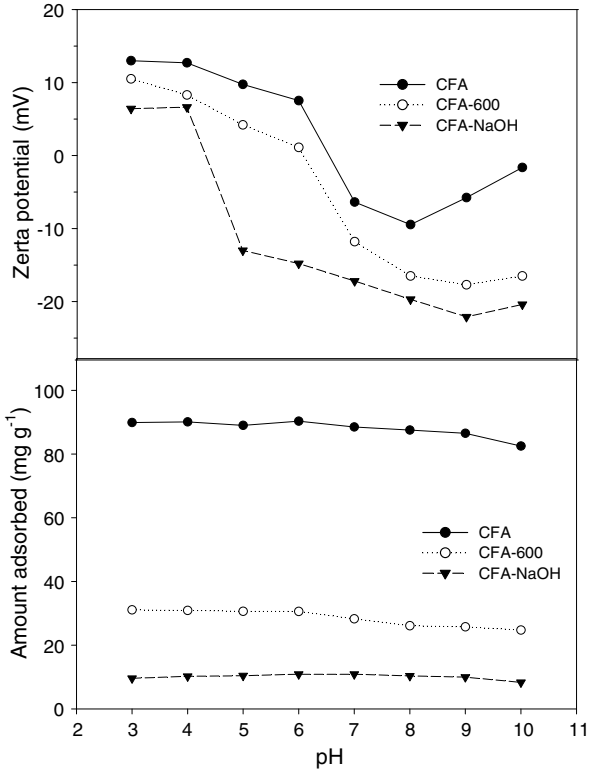

Fig. 2. Effect of pH and zeta potential on the adsorption of AR1 onto the three adsorbents at 30 °C.

pH 6, indicating that their ion-exchange processes would be difficult to perform.

Fig. 2 indicates that changing the pH of the solution from 3 to 10 had a slight effect on the adsorption of AR1 at a coal fly ash concentration of 1 g L^{-1} and an AR1 concentration of 400 mg L^{-1}. The adsorption capacities decreased slightly upon increasing the pH from 6 to 10. As the pH of the system increased, the number of negatively charged sites increased and the number of positively charged sites decreased. Negatively charged surface sites on the adsorbent did not favor the adsorption of the anionic dye because of electrostatic repulsion [7].

3.3. Effects of adsorbent and temperature

The adsorption experiments were performed at three different temperatures (30, 45, and 60 °C) using a concentration range of 0–400 mg/L for AR1 at a fixed pH (6.0) and contact time (180 min). Fig. 3 indicates that the adsorption capacities of the three adsorbents followed the order CFA > CFA-600 > CFA-NaOH at each temperature. We also found that the maximum adsorption capacity of AR1 occurred at 60 °C for each of the three adsorbents, with the adsorption capacities decreasing in the order 60 > 45 > 30 °C. The increase in the adsorption capacity upon increasing the temperature indicates that each adsorption was an endothermic process.

3.4. Dynamic adsorption studies

To investigate details of the adsorption processes of AR1 onto the three adsorbents, we analyzed the adsorption kinetics using several models, such as the pseudo-first-order Lagergren equation [5], a pseudo-second-order rate equation [25,26], and the intraparticle diffusion model [15], which are represented by Eqs. (2)–(4), respectively.

$$\ln(Q_e - Q_t) = \ln Q_e - k_1 t, \tag{2}$$

$$\frac{t}{Q_t} = \frac{1}{k_2 Q_e^2} + \frac{t}{Q_e}, \tag{3}$$

$$Q_t = k_i(t^{1/2}) + C, \tag{4}$$

where Q_t is the amount (mg g^{-1}) of material adsorbed at time t, Q_e is the adsorption capacity (mg g^{-1}) at equilibrium, k_1 is the rate constant (min^{-1}) of the pseudo-first-order model, k_2 is the rate constant (g mg^{-1} min^{-1}) of the pseudo-second-order model, k_i is the intraparticle diffusion rate constant (mg g^{-1} $min^{-0.5}$), C is the intercept (mg g^{-1}), and t is the time (min).

The experimental data for the different CFA samples were fitted using the pseudo-first-order, pseudo-second-order kinetics, and intraparticle diffusion models. Table 2 lists the parameters obtained using each of the models. The pseudo-first-order and intraparticle diffusion models did not represent the kinetics well; i.e., their regression coefficients were lower than those obtained using the second-order kinetics model (Fig. 4). The linearity of the plots of t/Q_t versus t (linear regression coefficients: >0.980) confirmed the pseudo-second-order nature of the process.

In the pseudo-second-order model, the product $k_2 Q_e^2$ is the initial sorption rate, h. Table 2 indicates that the pseudo-second-order rate constants (k_2) for CFA and CFA-600 had maximum values at 30 °C, whereas for CFA-NaOH it was maximized at 60 °C. The maximum initial sorption rates (h) for CFA, CFA-600, and CFA-NaOH were 24.938 mg g^{-1} min^{-1} (60 °C), 3.745 mg g^{-1} min^{-1} (30 °C) and 5.605 mg g^{-1} min^{-1} (60 °C), respectively.

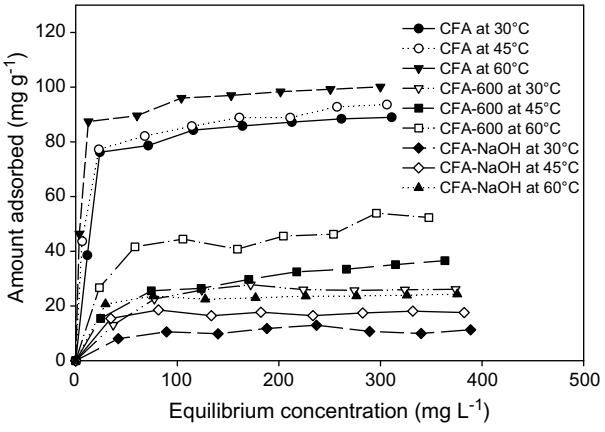

Fig. 3. Isotherms for the adsorption of AR1 onto CFA, CFA-600, and CFA-NaOH at various temperatures.

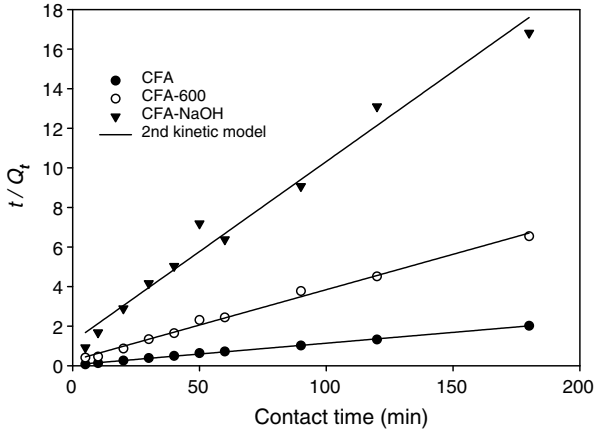

Fig. 4. Plots of pseudo-second-order kinetics for the adsorption of AR1 onto various CFA samples at 30 °C.

Table 2
Kinetic parameters of AR1 on CFA, CFA-600, and CFA-NaOH at various temperatures

Adsorbent	Temperature (°C)	Pseudo-first-order		Pseudo-second-order			Intraparticle diffusion	
		K_1 (1 min^{-1})	R^2	Q_e (mg g^{-1})	K_2 (g mg^{-1} min^{-1})	R^2	K_{i1} (K_{i2}) (mg g^{-1} $min^{-0.5}$)	R_1^2 (R_2^2)
CFA	30	0.381	0.962	91.743	0.003	0.998	25.712 (1.726)	0.948 (0.840)
	45	0.354	0.949	98.039	0.002	0.999	26.488 (2.114)	0.939 (0.878)
	60	0.394	0.949	104.167	0.002	0.999	28.293 (2.115)	0.923 (0.826)
CFA-600	30	0.162	0.950	27.933	0.005	0.994	5.500 (0.633)	0.946 (0.719)
	45	0.168	0.903	36.232	0.003	0.991	5.936 (1.072)	0.882 (0.762)
	60	0.064	0.881	59.880	0.001	0.991	6.819 (2.409)	0.886 (0.887)
CFA-NaOH	30	0.124	0.830	10.989	0.007	0.980	1.987 (0.429)	0.956 (0.772)
	45	0.118	0.870	17.857	0.006	0.975	2.980 (0.587)	0.944 (0.628)
	60	0.093	0.953	22.573	0.011	0.995	3.765 (0.909)	0.960 (0.605)

3.5. Adsorption isotherms

The adsorption equilibrium data for AR1 on the different adsorbents were fitted to both Langmuir and Freundlich isotherms [26,27]. The Langmuir isotherm is the most commonly used isotherm; it has been applied to analyze the sorption of a variety of compounds. In its linear form it can be represented as

$$\frac{1}{Q_e} = \frac{1}{Q_0} + \frac{1}{bQ_0C_e}, \tag{5}$$

where Q_e is the amount adsorbed (mg g^{-1}), C_e is the equilibrium concentration of the adsorbate (mg L^{-1}), and Q_0 and b are Langmuir constants related to the maximum adsorption capacity and the energy of adsorption, respectively. On the other hand, the Freundlich isotherm is most frequently used to describe the adsorption of inorganic and organic compounds from solution. In its logarithmic form it can be represented as

$$\log Q_e = \log K_F + \frac{1}{n}\log C_e, \tag{6}$$

where Q_e is the amount adsorbed (mg g^{-1}), C_e is the equilibrium concentration of the adsorbate (mg L^{-1}), and K_F (mg g^{-1}) and $n$are Freundlich constants related to the adsorption capacity and adsorption intensity, respectively. The values of Q_0, b, K_F, n, and the linear regression correlations for the Langmuir and Freundlich isotherms are given in Table 3. Because the regression coefficients (R^2) for the Langmuir and Freundlich isotherm were 0.906–0.991 and 0.833–0.979, respectively, it appears that the Langmuir model yielded a much better fit than the Freundlich model. For the three adsorbents, the maximum adsorption capacities (Q_0) at various temperatures decreased in the order 60 > 45 > 30 °C.

3.6. Thermodynamic studies

Table 4 lists the thermodynamic parameters calculated using the following equations [28]:

$$\Delta G^\circ = -RT\ln b', \tag{7}$$

$$\ln\left(\frac{b_2}{b_1}\right) = -\left(\frac{\Delta H^0}{R}\right)\left(\frac{T_1 - T_2}{T_2T_1}\right), \tag{8}$$

$$\Delta S^0 = \frac{\left(\Delta H^0 - \Delta G^0\right)}{T}, \tag{9}$$

where b', b_2, and b_1 are the Langmuir constants at T, T_2, and T_1, respectively. From Eq. (9), if ΔG° is plotted against T, a straight line is obtained having a slope of $-\Delta S^\circ$ and an intercept at ΔH°. In Table 4, the negative values of ΔG° at all temperatures indicate that the adsorption process is favorable and spontaneous. In addition, the free energy decrease upon increasing the temperature suggests that the process is favored at high temperatures. The positive values of ΔH° and ΔS° for each sample indicate that the adsorption process is both endothermic and aided by increased randomness. The increase in adsorption at higher temperatures also indicates the endothermic nature of these adsorption processes [29].

Table 4
Thermodynamic parameters for CFA, CFA-600, and CFA-NaOH

Adsorbent	ΔG° (kJ mol^{-1})			ΔH°	ΔS°	R^2
	30 °C	45 °C	60 °C	(kJ mol^{-1})	(J mol^{-1} K^{-1})	
CFA	−26.77	−28.17	−30.38	9.83	120.3	0.984
CFA-600	−23.18	−25.32	−27.82	23.74	154.7	0.998
CFA-NaOH	−25.03	−26.49	−28.76	12.79	124.4	0.985

3.7. Error analysis

In the single-component isotherm studies, the optimization procedure requires an error function to be defined to evaluate the fit of the isotherm and kinetics equation to the experimental equilibrium data. In this study, five different error functions were examined and in each case the isotherm and kinetic parameters were determined by minimizing the respective error function across the concentration range studied, using the solver add-in for Microsoft Excel 2003 [30,31]. The error functions studied were as follows:

3.7.1. Sum of the squares of the errors (ERRSQ)

The sum of the squares of the errors method can be represented by the equation

$$\sum_{i=1}^{p}(Q_{e,calc} - Q_{e,meas})_i^2, \tag{10}$$

where $Q_{e,calc}$ is the theoretical adsorbed solid phase concentration of AR1 on CFA, which was calculated from the equations represented by Eqs. (3) and (5), and $Q_{e,meas}$ is the experimentally determined adsorbed AR1 concentration obtained from Eq. (1) using the experimentally measured equilibrium AR1 liquid phase concentrations, C_e.

Although this error function is the most commonly used, it has one major drawback: Isotherm and kinetic parameters derived using this error function will provide a better fit as the magnitude of the errors and, thus, the squares of the errors increase, biasing the fit toward the data obtained at the high end of the concentration range.

3.7.2. Hybrid fractional error function (HYBRID)

This error function was developed [30,32] to improve the fit of the sum of the squares of the errors at low concentrations by dividing it by the measured value. It also includes the number of degrees of freedom of the system – the number of data points, n, minus the number of parameters, p, of the isotherm equation – as a divisor:

Table 3
Langmuir and Freundlich constants for CFA, CFA-600, and CFA-NaOH

Adsorbent	Temperature (°C)	Langmuir			Freundlich		
		Q_0 (mg g^{-1})	b (L mg^{-1})	R^2	n	K_F (mg g^{-1})	R^2
CFA	30	92.59	0.081	0.991	12.45	56.62	0.942
	45	96.15	0.083	0.919	11.60	57.00	0.964
	60	103.09	0.115	0.980	15.55	69.82	0.916
CFA-600	30	32.79	0.020	0.906	3.39	4.97	0.897
	45	37.31	0.028	0.981	3.26	6.13	0.970
	60	52.63	0.045	0.919	4.65	14.98	0.833
CFA-NaOH	30	12.66	0.041	0.942	7.04	4.85	0.967
	45	19.76	0.044	0.945	14.58	12.40	0.934
	60	25.12	0.064	0.963	14.16	15.96	0.979

$$\frac{100}{n-p}\sum_{i=1}^{n}\left(\frac{(Q_{e,meas}-Q_{e,calc})^2}{Q_{e,meas}}\right)_i. \quad (11)$$

3.7.3. Marquardt's percent standard deviation (MPSD)

This error function [33] has been used previously by several researchers in the field [34,35]. It is similar in some respects to a geometric mean error distribution, modified according to the number of degrees of freedom of the system:

$$100\sqrt{\frac{1}{n-p}\sum_{i=1}^{p}\left(\frac{Q_{e,meas}-Q_{e,calc}}{Q_{e,meas}}\right)_i^2}. \quad (12)$$

3.7.4. Average relative error (ARE)

This error function [36] attempts to minimize the fractional error distribution across the entire concentration range:

$$\frac{100}{n}\sum_{i=1}^{p}\left|\frac{Q_{e,calc}-Q_{e,meas}}{Q_{e,meas}}\right|_i. \quad (13)$$

3.7.5. Sum of absolute errors (EABS)

This approach is similar to the sum of the squares of the errors. Isotherm and kinetic parameters determined using this error function would provide a better fit if the magnitude of the error increases the bias of the fit toward the high concentration data.

$$\sum_{i=1}^{p}|Q_{e,calc}-Q_{e,meas}|_i. \quad (14)$$

Because all of the experiments were performed at mass-to-volume ratios that almost exactly described in terms of units of g L^{-1}, according to the formulation of the problem, both C_e and Q_e contribute equally to weighting the error criterion for the model solution procedure. Hence, the difference in the sorbed phase concentration reflects the differences in the predicted concentration for both phases. In Figs. 5 and 6, when the errors were normalized for comparison, the ARE and EABS error function methods provided the best parameters for the Langmuir isotherm and the pseudo-second-order equation, respectively, in the AR1–CFA adsorption system. Table 5 provides the error analyses for the Langmuir isotherm and pseudo-second-order kinetics of AR1 onto CFA at various temperatures. The ARE and EABS methods have the highest values of R^2 among the various error function methods and, therefore, are more significant. These data will be used in the design of commercial adsorbers and, consequently, the more accurate the isotherm and kinetics equation parameters, the more accurate will be the system design [30,31].

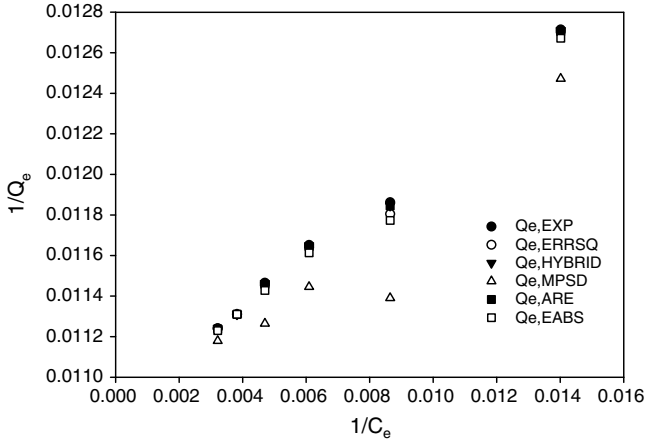

Fig. 5. Langmuir isotherm plots for the adsorption of AR1 onto CFA at 30 °C using various methods of error analysis.

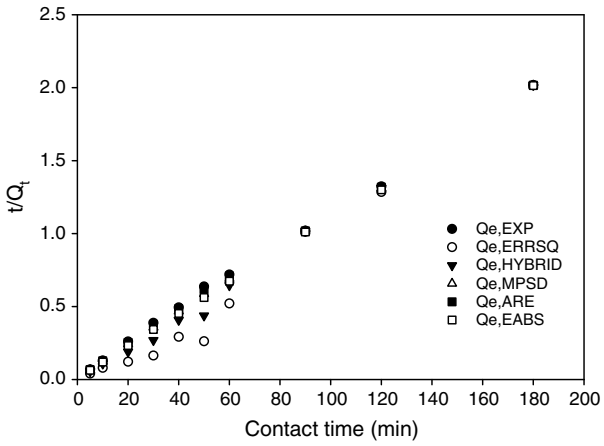

Fig. 6. Pseudo-second-order kinetics for the adsorption of AR1 onto CFA at 30 °C using various error analysis methods.

Table 5
Analysis of the single-component Langmuir isotherm and pseudo-second-order kinetics for the adsorption of AR1 onto CFA using various error functions

	ERRSQ	HYBRID	MPSD	ARE	EABS
Langmuir isotherm					
30 °C					
Q_0 (mg g^{-1})	92.59	92.59	92.59	92.59	92.59
b (L mg^{-1})	0.082	0.081	0.098	0.081	0.084
R^2	0.983	0.989	0.868	0.990	0.982
45 °C					
Q_0 (mg g^{-1})	99.01	96.15	97.09	96.15	97.09
b (L mg^{-1})	0.072	0.080	0.080	0.083	0.080
R^2	0.969	0.956	0.949	0.930	0.964
60 °C					
Q_0 (mg g^{-1})	103.10	103.10	103.10	103.10	103.10
b (L mg^{-1})	0.118	0.115	0.117	0.115	0.119
R^2	0.961	0.976	0.973	0.978	0.966
Pseudo-second-order kinetics					
30 °C					
Q_0 (mg g^{-1})	85.47	87.72	90.91	90.91	90.91
k_2 (g mg^{-1} min^{-1})	−0.001	−0.003	0.006	0.003	0.014
R^2	0.980	0.996	0.999	0.999	1.000
45 °C					
Q_0 (mg g^{-1})	94.34	96.15	98.04	98.04	98.04
k_2 (g mg^{-1} min^{-1})	−0.013	0.006	0.003	0.002	0.003
R^2	0.997	0.998	0.999	0.999	0.999
60 °C					
Q_0 (mg g^{-1})	100.00	102.04	103.09	103.09	103.09
k_2 (g mg^{-1} min^{-1})	−0.008	0.007	0.003	0.003	0.004
R^2	0.999	0.998	0.998	0.999	0.999

4. Conclusions

Even without pretreatment, coal fly ash, a solid waste obtained from coal-burning power plants, is a cheap and effective adsorbent for the removal of AR1 from water. Changing the nature of the raw coal fly ash through heating or modification with NaOH solution did not improve its ability to adsorb AR1. According to dynamic and thermodynamic studies, each of these adsorption processes was endothermic and followed pseudo-second-order kinetics. The adsorptions of AR1 onto the raw and modified coal fly ashes fit the Langmuir isotherm very well; the adsorptions capacities of CFA, CFA-600, and CFA-NaOH toward AR1 were 92.59–103.09, 32.79–52.63, and 12.66–25.12 mg g^{-1}, respectively. From a study

of various error analysis approaches, the ARE and EABS error function methods provided the best parameters for the Langmuir isotherm and the pseudo-second-order equation, respectively, for the AR1–CFA adsorption system.

References

[1] Accmioglu B. Adsorption of Congo red from aqueous solution onto calcium-rich fly ash. J Colloid Interf Sci 2004;274:371–9.
[2] Wang SB, Zhu ZH. Characterisation and environmental application an Australian natural zeolite for basic dye removal from aqueous solution. J Hazard Mater 2006;136:946–52.
[3] Gupta VK, Mittal A, Krishnan L, Gajbe V. Adsorption kinetics and column operations for the removal and recovery of malachite green from wastewater using bottom ash. Sep Purif Technol 2004;40:87–96.
[4] Wang CC, Juang LC, Hsu TC, Lee CK, Lee JF, Huang FC. Adsorption of basic dyes onto montmorillonite. J Colloid Interf Sci 2004;273:80–6.
[5] Wang SB, Li H. Dye adsorption on unburned carbon: kinetics and equilibrium. J Hazard Mater 2005;126:71–7.
[6] Janos P, Buchtova H, Ryznarova M. Sorption of dye from aqueous solution onto fly ash. Water Res 2003;37:4938–44.
[7] Mall ID, Srivastava C, Agarwa NK. Removal of Orange-G and Methyl Violet dyes by adsorption onto bagasse fly ash – kinetic study and equilibrium isotherm analyses. Dyes Pigments 2006;69:210–23.
[8] Wang SB, Wu H. Environmental-benign utilization of fly ash as low-cost adsorbents. J Hazard Mater 2006;136:482–501.
[9] Wang SB, Boyjoo Y, Choueib A, Zhu ZH. Removal of dyes from aqueous solution using fly ash and red mud. Water Res 2005;39:129–38.
[10] Gupta VK, Ali I, Saini V K, Gerven TV, Van der Bruggen B, Vandecasteele C. Removal of dyes from wastewater using bottom ash. Ind Eng Chem Res 2005;44:3655–64.
[11] Gupta VK. Removal and recovery of the hazardous azo dye Acid Orange 7 through adsorption over waste materials: bottom ash and de-oiled soya. Ind Eng Chem Res 2005;44:3655–64.
[12] Gupta VK, Mohan D, Sharma S, Sharma M. Removal of basic dyes (rhodamine B and methylene blue) from aqueous solutions using bagasse fly ash. Sep Sci Technol 2000;35:2097–133.
[13] Chander M, Arora DS. Evaluation of some white-rot fungi for their potential to decolourise industrial dyes. Dyes Pigments 2007;72:192–8.
[14] Robinson T, Chandran P, Nigam P. Removal of dyes from a synthetic textile dye effluent by biosorption on apple pomace and wheat straw. Water Res 2002;36:2824–30.
[15] Gong R, Jin Y, Chen J, Hu Y, Sun J. Removal of basic dye from aqueous solution by sorption on phosphoric acid modified rice straw. Dyes Pigments 2007;73:332–7.
[16] Tsai WT, Chang CY, Lin MC, Chien SF, Sun HF, Hsieh MF. Adsorption of acid dye onto activated carbon prepared from agricultural waste bagasse by $ZnCl_2$ activation. Chemosphere 2001;45:51–8.
[17] Namasivayam C, Kavitha D. Removal of Congo Red from water by adsorption onto activated carbon prepared from coir pith, an agricultural solid waste. Dyes Pigments 2002;54:47–58.
[18] Mittala A, Krishnana L, Gupta VK. Removal and recovery of malachite green from wastewater using an agricultural waste material, de-oiled soya. Sep Purif Technol 2005;43:125–33.
[19] Gupta VK, Ali I, Saini VK. Adsorption studies on the removal of Vertigo Blue 49 and Orange DNA13 from aqueous solutions using carbon slurry developed from a waste material. J Colloid Interf Sci 2007;315:87–93.
[20] Gupta VK, Suhas, Ali I, Saini VK. Removal of rhodamine B, fast green, and methylene blue from wastewater using red mud, an aluminum industry waste. Ind Eng Chem Res 2004;43:1740–7.
[21] Jain AK, Gupta VK, Bhatnagar A, Suhas. Utilization of industrial waste products as adsorbents for the removal of dyes. J Hazard Mater 2003;101:31–42.
[22] Gupta VK, Ali I, Suhas, Mohan D. Equilibrium uptake and sorption dynamics for the removal of a basic dye (basic red) using low-cost adsorbents. J Colloid Interf Sci 2003;265:257–64.
[23] Wang J, Teng X, Wang H, Ban H. Characterizing the metal adsorption capability of a class F coal fly ash. J Environ Sci Technol 2004;38:6710–5.
[24] Hsu TC, Yu CC, Yeh CM. Adsorption of Cu^{2+} from water using raw and modified coal fly. Fuel 2008;87:1355–9.
[25] Wang CC, Juang LC, Lee CK, Hsu TC, Lee JF, Chao HP. Effect of exchanged surfactant cations on the pore structure and adsorption characteristics of montmorillonite. J Colloid Interf Sci 2004;280:27–35.
[26] Juang LC, Wang CC, Lee CK. Adsorption of basic dyes onto MCM-41. Chemosphere 2006;64:1920–8.
[27] Juang LC, Wang CC, Lee CK, Hsu TC. Dye Adsorption onto organoclay and MCM-41. J Environ Eng Manage 2007;17:29–38.
[28] Gupta VK, Ali I. Removal of lead and chromium from wastewater using bagasse fly ash – a sugar industry waste. J Colloid Interf Sci 2004;271:321–8.
[29] Sawyer CN, McCarty PL, Parkin GF. Chemistry for environmental engineering and science. 5th ed. New York: McGraw-Hill; 2003. p. 58.
[30] Ng JCY, Cheung WH, McKay G. Equilibrium studies of the sorption of Cu(II) ions onto chitosan. J Colloid Interf Sci 2002;255:64–74.
[31] Rengaraj S, Yeon JW, Kim Y, Jung Y, Ha YK, Kima WH. Adsorption characteristics of Cu(II) onto ion exchange resins 252H and 1500H: kinetics, isotherms and error analysis. J Hazard Mater 2007;143:469–77.
[32] Porter JF, McKay G, Choy KH. The prediction of adsorption from binary mixture of acidic dyes using single- and mixed-isotherm variants of the ideal adsorbed solute theory. Chem Eng Sci 1999;54:5863–85.
[33] Marquardt DW. An algorithm for least-squares estimation of nonlinear parameters. J Soc Ind Appl Math 1963;11:431–41.
[34] Seidel A, Gelbin D. On applying the ideal adsorbed solution theory to multicomponent adsorption equilibria of dissolved organic components on activated carbon. Chem Eng Sci 1988;43:79–89.
[35] Seidel-Morgenstern A, Guiochon G. Modelling of the competitive isotherms and the chromatographic separation of two enantiomers. Chem Eng Sci 1993;48:2787–97.
[36] Kapoor A, Yang RT. Correlation of equilibrium adsorption data of condensable vapours on porous adsorbents. Gas Sep Purif 1989;3:187–92.